Microfluid Nanofluid
DOI 10.1007/s10404-014-1389-8

RESEARCH PAPER

Simplified analysis method of cell-free layers in blood flows as tool for the optimization of gas exchange devices

Tina Rieper · Paul Čvančara · Claas Müller · Holger Reinecke

Received: 9 December 2013 / Accepted: 22 March 2014

Abstract A novel analyzing method is presented, which allows precise characterization of cell-free layers (CFLs) of blood flowing through microchannels. The CFL occurs due to axial migration of the erythrocytes (RBCs). A confocal laser scanning microscope (CLSM) is used to detect the reflected light of channel walls and cells within the blood flow. Since the presented method does not depend on emitted fluorescence signals, there is no necessity for a complex sample preparation as fluorescence marking of cells. Furthermore, it allows the characterization of the thickness of the CFL in whole blood. Due to the high vertical resolution of the used CLSM, the developed characterization method enables measurements along the optical axis of the microscope. It is exemplarily used to analyze the thickness of the CFL in human blood flowing through microchannels as a function of the hematocrit and blood flow velocity. The microchannels are made of silicone rubber with a height of 100 µm. The microchannels are intended for a gas exchange application.

Keywords Cell-free layer · Blood flow · Microchannels · Confocal laser scanning microscope

1 Motivation

When developing an extracorporeal gas exchange device (EGED), as applied in the extracorporeal membrane oxygenation (ECMO), one needs to avoid a cell-free layer (CFL) in the flowing blood since it reduces the transfer efficiency of the EGED. Within an EGED diffusive gas exchange between a gas compartment and a blood compartment, mainly the RBCs within, takes place. A schematic cross-section through one of the microchannels of the EGED concept developed by Rieper et al. (2012a) is shown in Fig. 1. Axial migration of the RBCs toward the channel center would lead to an increased flow velocity of the RBCs as the fluid flow velocity in the channel center is higher. Therefore, the retention time of the RBCs within the gas exchange device decreases. A further disadvantage is that the diffusion length for the gases from the diffusion membrane to the RBCs increases, due to the diffusion path of the gases along the axial z-direction (Rieper et al. 2012b). The influence of the CFL on the gas exchange is particularly high if the CFL occurs not only at the channel side walls but at the bottom and the top of the channel. For these reasons, the microchannels of the EGED have to be optimized with respect to a reduced CFL. Here, the thickness of the occurring CFL is of main interest and not the exact distribution of RBCs within the flow. According to theory, a CFL within the microchannels of the gas exchange device is expected since the influence of the RBCs (diameter of 7–8.5 µm) (Campbell and Reece 2002) on the fluid flow within a channel of 100 µm height can't be neglected. Therefore, the flow drives the RBCs toward the channel center. The CFL will decrease with rising hematocrit (*hct*) (Lima et al. 2009; Cerdeira et al. 2009) and increase with higher blood flow velocity v. For these reasons, the thickness of the CFL occurring in the above-mentioned EGED is investigated by means of an evaluation model of the EGED. Hence, a new analysis method was developed, which allows a characterization of the CFL in the axial z-direction with no need of a special sample preparation and therefore lowering the laboratory effort.

T. Rieper (✉) · P. Čvančara · C. Müller · H. Reinecke
Laboratory for Process Technology, Department of Microsystems Engineering - IMTEK, University of Freiburg, Georges-Koehler-Allee 103, 79110 Freiburg, Germany
e-mail: tina.rieper@imtek.uni-freiburg.de; tina.rieper@imtek.de

Published online: 05 April 2014

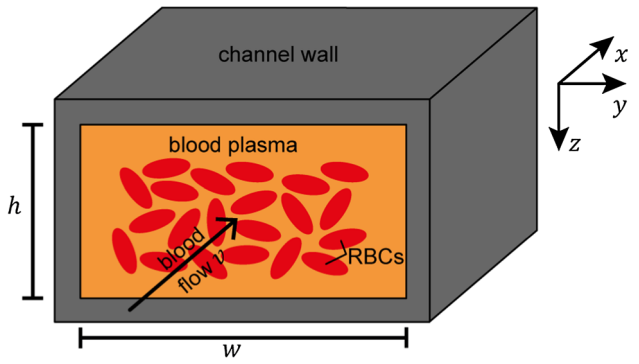

Fig. 1 Schematic cross-section through blood flowing within a microchannel of the evaluation model in direction of *x*. Due to the axial migration, the RBCs move toward the channel center and a CFL occurs at the channel walls. Furthermore, the orientation of the axis is shown on the *right*

The axial *z*-direction is of special interest as not only its influence on the gas exchange is highest but also as the CFL is thicker along the axial *z*-direction. This is true, due to the larger velocity profile curvature, if the channel width *w* is larger than the channel height *h*, as it is the case for the EGED. For the application as EGED, the CFL only in whole blood is of interest. To show a more general applicability, a hematocrit range of 20 % to 44 % (physiological human hematocrit) is investigated.

2 Theory

If a suspension flows in the laminar regime through a microchannel, migration of the solid particles toward the channel center to an equilibrium position might occur. Segré and Silberberg (1962) identified this equilibrium position for tubular microchannels in Newtonian fluid flows at approximately 60 % of the distance from the tube center line to the tube wall for neutrally buoyant rigid spheres. This behavior is known as Segré–Silberberg effect. The migration of particles across the streamlines of the flow, also known as axial migration, occurs in the presence of walls, a velocity profile curvature and buoyancy forces, unless the particle is so small that its relative motion with respect to the fluid is negligible (Karnis et al. 1966). As driving forces a wall repulsion due to lubrication, an inertial lift related to shear slip, a lift due to particle rotation and in Pouseuille flow a lift caused by the velocity profile curvature were identified (Feng et al. 1994). The exact location of the radial equilibrium position depends mainly on the channel geometry, the channel surface, the flow velocity and characteristics of the suspension, like e.g., the viscosity, the particle size and the solid fraction. The axial migration might lead to a particle depleted or particle free layer at the channel wall.

Axial migration is a known effect in flowing blood and results in the Fåhræus–Lindqvist effect, which describes the lowering of the apparent viscosity of blood flowing through channels or tubes with dimensions below approximately 300 µm (Fahraeus and Lindqvist 1931). CFLs might occur at the channel walls as a result of the RBC migration to the channel center.

3 Materials

3.1 Evaluation model

Along with the flow characteristics, the CFL is influenced by the channel characteristics. Therefore, the thickness of the CFL is analyzed in an evaluation model with microchannels of the same cross-section ($w \times h$: 1 mm × 0.1 mm) and the same material (silicone rubber; *Elastosil® RT601*, Wacker Chemie AG, München, Germany) as the EGED. To guarantee the same surface characteristics, the evaluation models are fabricated in the same way as the EGED (Rieper et al. 2013). A silicone rubber sheet showing the structures of the microchannels is fabricated by casting a ultra precision machined tool. A 50-µm-thick silicone rubber cover sheet is fabricated by casting a polished, unstructured tool plate. The cover sheet is bonded to the structured sheet by curing an approximately 5-µm-thick silicone rubber inter layer applied on the structured sheet before covering with the cover sheet. The connectors are also casted and then bonded by an uncured silicone rubber inter layer to the sheet assembly. For the characterization of the CFL, the cover sheet of the evaluation model is reinforced with glass cover slips to avoid bowing of the cover sheet due to the blood flow. The cover slips are full-faced bonded to the evaluation model also by curing a silicone rubber inter layer. The evaluation model, shown in Fig. 2, consists of ten parallel, 100 mm long (*l*) microchannels which are separated from each other by 0.5 mm wide bars. Fig. 3 depicts the cross-section of one

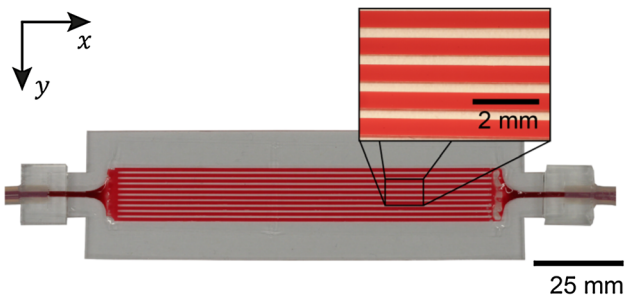

Fig. 2 Evaluation model for the characterization of the CFL thickness with ten parallel microchannels (0.1 mm high and 1 mm wide) filled with human whole blood. The blood flow direction (*x*-direction) through the evaluation model is from the *left* to the *right*

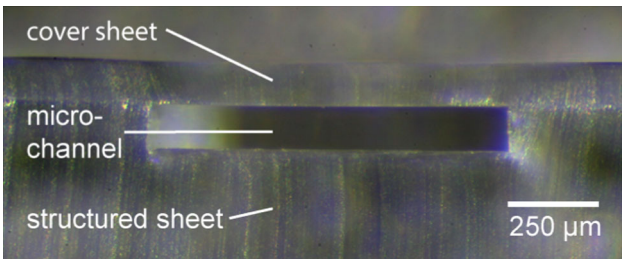

Fig. 3 Cross-section through one of the ten parallel microchannels of the evaluation model

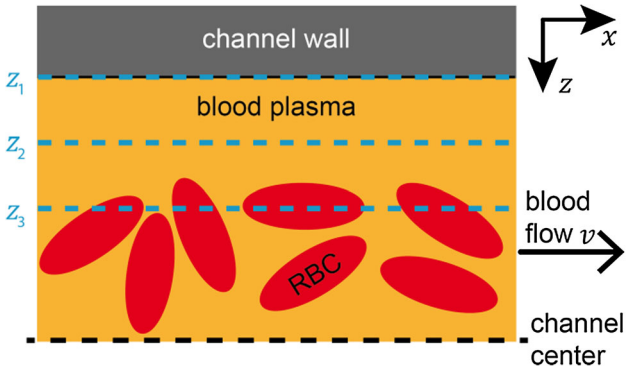

Fig. 4 Schematic detail of the microchannel cross-section showing a CFL due to axial migration of the *red* blood cells

microchannel fabricated in silicone rubber covered with a 100-µm-thick cover sheet.

3.2 Blood

Anticoagulated human blood is derived by venipuncture with EDTA-monovettes (*S-Monovette®, Sarstedt*). The initial hematocrit measurements are performed with a photometer (*Hemo_Control, EFK diagnostic GmbH*). If necessary, the blood is diluted to the desired hematocrit with isotonic saline and stored in a glass reservoir. During storage, the blood sample is slightly stirred to prevent cell sedimentation and the temperature is controlled to be 37 °C. Blood samples were rejected latest 4 h after the venipuncture.

4 Analysis method

In literature, different methods of analyzing a CFL or the distribution of RBCs in blood flows within microchannels are presented. One method is the microparticle image velocimetry (µPIV) (Lima et al. 2008). Hereby, fluorescent particles, like fluorescence marked RBCs or fluorescent microspheres, added to the blood, are traced, and hence, their velocity calculated to obtain a flow profile. Furthermore, the distribution of the marked particles can be determined. A disadvantage of this method is the restricted applicability to low hematocrits as the observed signal intensity decreases with increasing hematocrit, due to shadowing effects. The second method was presented by Park et al. (2006). Park et al. reported that blood flows with a hematocrit in the range of 10 % to 40 % and a velocity between 1.67 mm/s and 20 mm/s cannot be analyzed in 50 µm × 50 µm silicone rubber channels with µPIV. Instead, Park et al. used an optical microscope equipped with a high speed camera to take snapshots of the blood flow. Those snapshots were used to measure the CFL at the channel side walls. De Tilly et al. (2010) tracked unmarked RBCs in undiluted whole blood flows with a high speed camera. However, the last two described methods can only be used to characterize the blood flow in the lateral observation plane (*xy*) and not orthogonal to it as necessary in the case of the EGED. Reason therefor is the low resolution in direction of the optical axis (*z*).

The developed method of analyzing the thickness of the CFL with a confocal laser scanning microscope is based on reflection of the laser light at interfaces within the evaluation model. Such reflection sites are the interface between the diffusion membrane and the blood flow (z_1 in Fig. 4) and the cells or other particles within the flow (z_3 in Fig. 4). To gain the highest intensity of the reflected signal of the RBCs, the laser source of the CLSM emitting a wavelength of 633 nm is chosen. The laser scans the focal plane (*xy*) in *y*-direction bidirectionally line by line. Such scans are performed at different *z*-positions resulting in a *z*-stack of scans for each parameter set to be analyzed. The step size between the scans is optimized to increase the vertical resolution of the CFL analysis. As a trade-off between measuring time and vertical resolution the optimal step size was identified to be half the depth of focus (DOF = 0.6 µm). If the focal plane is equal to the membrane–blood interface (z_1 in Fig. 4), the light is reflected due to the difference in refraction indices and the reflected signal is detected in the whole plane by the CLSM image sensor. The result is a scan with all pixels having values ≥ 1 (z_1 in Fig. 5). If the focal plane is within the CFL (z_2 in Fig. 4), no reflection occurs as there are no RBCs or larger particles. Therefore, no signal is detected and all pixels of the scan have the value 0 (z_2 in Fig. 5). If there are RBCs in the focal plane (z_3 in Fig. 4), reflected signals from RBCs will be detected. Due to the line-by-line scanning of the microscope and the flow velocity of the RBCs, each cell will be detected in only one line of the scan and result in a line of differing length with pixels of a value ≥ 1 (z_3 in Fig. 5). At the time the laser reaches the former cell position (*y*) in the next line again, the cell will already have exited the scanning area. The color gradient in the scan of the membrane–blood interface (z_1 in Fig. 5 bottom) results

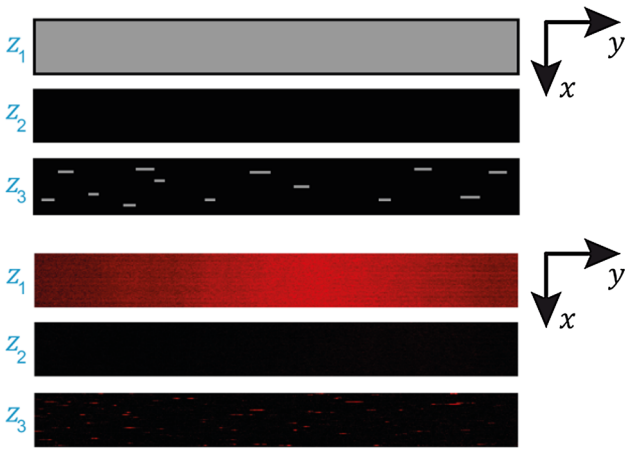

Fig. 5 Scans in the different planes of interest while blood is flowing in x-direction. *Top*: Schematics of the binarized scans. Pixels with a *gray* level of 0 occur *black*. Pixels with values ≥ 1 occur *gray*. *Bottom*: Original scans for $hct = 20$ %. The color gradient in z_1 is due to a slight tilting of the evaluation model on the microscope stage

from a slight tilting of the evaluation model on the microscope stage. To reduce the influence of the tilting of the evaluation model, only a section around the center point of all scans with 1/10 of the scan width is evaluated.

5 Signal processing

For the CFL analyzes, the scans are processed with the freely available software *ImageJ* as follows. First, the original scans (see Fig. 5 bottom) are transferred to gray scale. Corresponding to the originally detected signal intensity, all pixels have gray levels (gl) between 0 and 255. Next, the scans are binarized, leading to gl of the pixels of either zero or one. The threshold value is optimized for a reduction of background noise and varies due to the illumination settings for each experiment. Single pixels with $gl = 1$, only neighbored by pixels with $gl = 0$, are eliminated using a median filter, a nonlinear digital filtering technique, in order to reduce the influence of measurement artifacts.

The scan signal, i.e., the amount of pixels with $gl = 1$, at the intersection of CFL and blood with RBCs is very low, due to the small area of the scanned RBCs. To improve the observability of these regions, an optimized amount of 20 binarized and filtered scans of the same plane is added up to one image. Due to the adding of the scans, the method becomes more stable against measurement artifacts as a consequence of single pathologic cells or other particles within the CFL, as not only one scan showing a rare artifact is evaluated.

Finally, the added image is used to evaluate the CFL. Therefore, the percentage of pixels with a $gl \geq 1$

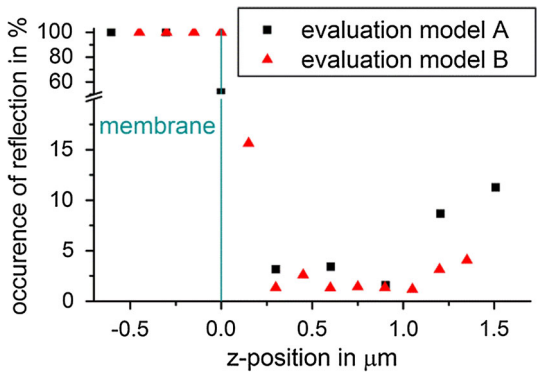

Fig. 6 Plot of the occurrence of reflection over the z-position for the case of no detectable CFL. The results correspond to two measurements performed with two different evaluation models (A and B). The parameters for these measurements were $hct = 30$ % and $v = 234$ mm/s

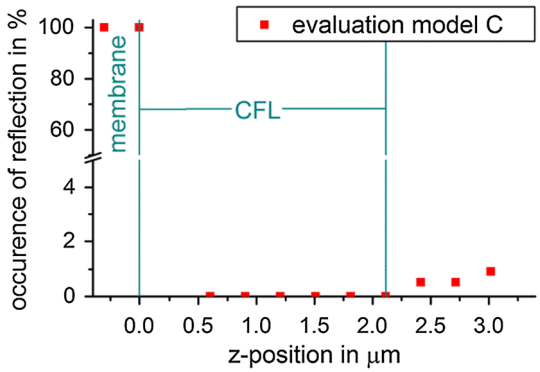

Fig. 7 Plot of the occurrence of reflection over the z-position for the case of a detectable CFL of 2.1 µm thickness. The parameters for this measurement were $hct = 20$ % and $v = 234$ mm/s

(occurrence of reflection) is calculated for each sum image. Distributions comparable to those in Figs. 6 and 7 are derived by plotting the occurrence of reflection over the z-position of a scan. The maximum z-position where the occurrence is >50 % is set to zero and marks the interface between diffusion membrane and blood flow. If there is no detectable CFL, the occurrence will not decline to zero (see Fig. 6). If there is a CFL, the occurrence will decline to zero over the whole thickness of the CFL (see Fig. 7). The occurrence will increase to a value related to the hematocrit as soon as there are RBCs in the scanned plane. The thickness of the CFL is derived by evaluating the z-range with an occurrence of zero.

It should be noted that the occurrence of reflection must not be understood as the RBC density as signals reflected of several RBCs might overlap due to the summation of 20 scans, and the amount of pixels with $gl \geq 1$ per RBC varies with the blood flow velocity. With the presented method, therefore, only the occurrence and thickness of a CFL can be detected and not the distribution of RBCs within the flow.

6 Experimentals

The CFL thickness (d_{CFL}) is characterized in dependency of the hematocrit and the blood flow velocity. The parameter ranges are shown in Table 1. The experimental setup incorporating a *LSM 510 Meta* (Zeiss, Oberkochen, Germany) as CLSM is depicted in Fig. 8. The CLSM is an upright microscope and its settings are summarized in Table 2. All analyzes are performed at a x-position behind the channel entrance ($x \geq 40$ mm) far enough to ensure a fully developed flow profile. Therefore, the CFL may vary from experiment to experiment due to local artifacts in the microchannel. The blood is pumped through the evaluation model by a software controlled syringe pump *neMESYS* (cetoni GmbH, Korbußen, Germany). The blood flow velocity given in the following is the mean blood flow velocity and is adjusted by the volume flow rate. The transversion of volume flow to blood flow velocity is calculated considering the actual geometry of each microchannel. All evaluation models used in this study (A, B, C, D, E, F, G) were fabricated in the same way with the same tools and the same product charge of silicone rubber. Potential geometry deviations between the evaluation models result from fabrication tolerances, e.g., during the bonding process. To avoid an influence of contaminations and surface variations within the microchannels, e.g., due to protein deposition, for each experiment day a new evaluation model was used in general. The evaluation models B and D were analyzed with different blood samples to investigate the influence of the blood sample after extensively rinsing them with isotonic saline solution, ethanol and deionized water and drying them in a furnace at 80 °C for 1 h.

Table 1 Parameters for which the CFL thickness is characterized

Parameter	Analyzed values
Hematocrit *hct*	20; 25; 30; 44 %
Blood flow velocity *v*	33; 67; 100; 134; 167; 200; 234 mm/s

Table 2 Settings of the CLSM (*LSM 510 Meta*, Zeiss, Germany)

Parameter	Value
Wavelength	633 nm
Laser intensity	28 %
Pin hole	46 µm
Objective	63×
Numerical aperture	1.2
Immersion medium	Deionized water
Depth of focus	0.6 µm
Gain	500–655 (depending on the exact membrane thickness)
Scan area	12 µm × 133.6 µm
Pixel size	0.062 µm^2
Recording duration per pixel	2.56 µs

Geometry deviations between the evaluation models caused by fabrication tolerances, hematocrit variations due to dilution errors and specific characteristics of one blood sample like plasma viscosity and RBC deformability which might differ for each proband and blood sample have a distinct influence on the blood flow profile and hence the CFL thickness. Consequently, comparability measurements with a standard parameter set ($v = 234$ mm/s, $x = 85$ mm) were performed for each experiment and the according hematocrit. If necessary, the analysis of the standard parameter set (comparability experiments) was used to normalize each experiment. This leads to a comparability between the experiments independent of the used evaluation model or especially the blood sample.

7 Results

The resolution of the measurement results is limited due to the depth of focus of 0.6 to ±0.3 µm. The precision was evaluated by analyzing the CFL thickness for the same parameter set ($v = 234$ mm/s and $hct = 20$ %) and the same evaluation model (D) five times. The hematocrit of

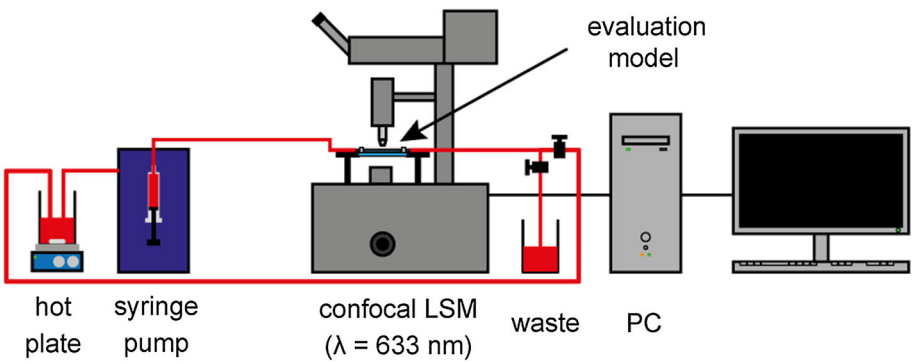

Fig. 8 Schematic of the experimental setup. The evaluation model is mounted on the stage of the CLSM. A syringe pump drives the blood through the evaluation model with a constant velocity. The CLSM is computer controlled

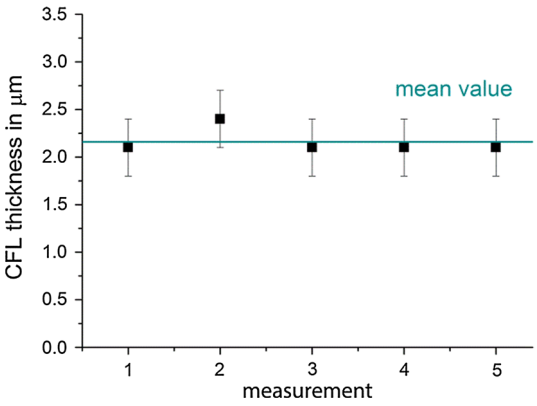

Fig. 9 Results of the five precision measurements with evaluation model D. The mean thickness $\overline{d_{\mathrm{CFL}}}$ is 2.1 µm. The *error bars* correlate to the depth of focus (±0.3 µm)

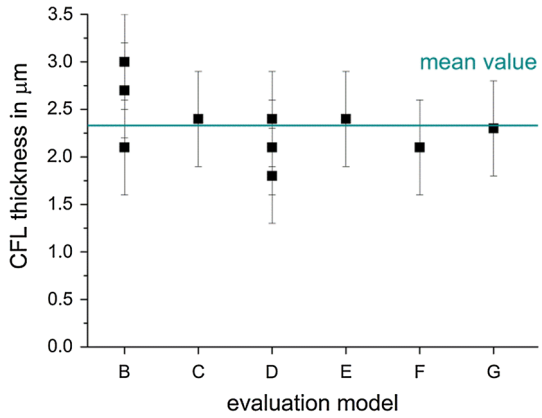

Fig. 10 Results of the comparability measurements with the standard parameter set for $hct = 20$ % for all evaluation models used in this study. Evaluation models with more than one data point were measured on different days with different blood samples after an extensive rinsing

20 % was chosen since it is more challenging to analyze than a higher hematocrit due to the lower signal density. The mean value of the CFL thickness $\overline{d_{\mathrm{CFL}}}$ is 2.1 µm; the range is $\overline{d_{\mathrm{CFL}}}^{+0.2\mu m}_{-0.1\mu m}$. The results are shown in Fig. 9. The reproducibility of the measurements was characterized with the same parameter set, but in between each of five experiments, the evaluation model (B) was demounted and mounted again on the microscope stage. The mean value of the CFL thickness for these experiments $\overline{d_{\mathrm{CFL}}}$ is 2.9 µm; the range is $\overline{d_{\mathrm{CFL}}}^{+0.1\mu m}_{-0.2\mu m}$. No distinct influence of the handling on the characterization of the CFL thickness was detected. The variation of the mean values of the CFL thicknesses is caused by the influence of the evaluation model and the blood sample. Due to these influences, the normalization of each measurement using the comparability experiment becomes necessary. Corresponding to the values, the error bar for the following measurement results is ±0.5 µm (half of the depth of focus plus the one-sided maximum of the range for the precision measurements).

Figure 10 shows the result of the comparability measurements with the standard parameter set for $hct = 20$ %. It can be seen that the measured CFL thicknesses for evaluation model B, used for the reproducibility measurement, are in general slightly higher than those measured for evaluation model D, used for the precision measurement. Furthermore, the influence of different blood samples from different probands, which will mainly differ in their plasma viscosity and RBC deformability, is shown for evaluation model B and D. The reader should note that the deviation of the CFL thickness is within the determined error of the method, except for two outliers during the repeated characterization of evaluation models B and D which may be due to contaminations or surface changes as a result of the repeated usage.

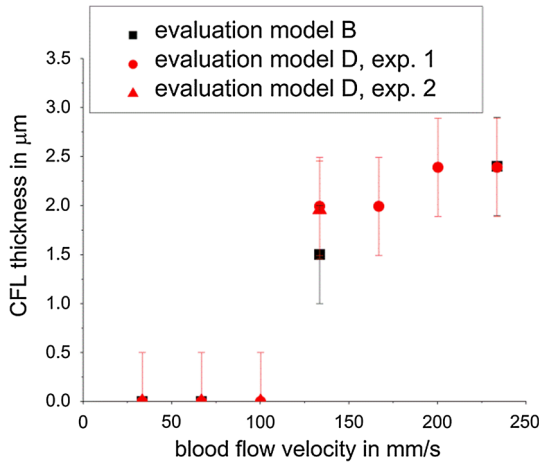

Fig. 11 Thickness of the CFL depending on the blood flow velocity for $hct = 20$ %. Three measurements, one with evaluation model B and two measurements with evaluation model D with two different blood samples, are depicted

For $hct = 20$ %, no CFL is detected for blood flow velocities up to 100 mm/s. The maximum CFL thickness of 2.4 µm is detected for a blood flow velocity of 234 mm/s. The results for three experiments are shown in Fig. 11. The characterization of the CFL thickness for $hct = 25$ % showed no detectable CFL for blood flow velocities up to 134 mm/s. The maximum CFL thickness of 1.5 µm is detected for a blood flow velocity of 234 mm/s (see Fig. 12). No CFL was detected for hct = 30 % (see Fig. 6) or higher, even with a blood flow velocity of 234 mm/s. For these parameters, the occurrence of reflection is >1 % for each z-position. Within the evaluation model, no distinct CFL occurs for a physiological hematocrit ($hct = 44$ %) and the analyzed blood flow velocities, which are by far higher than the one used in the gas

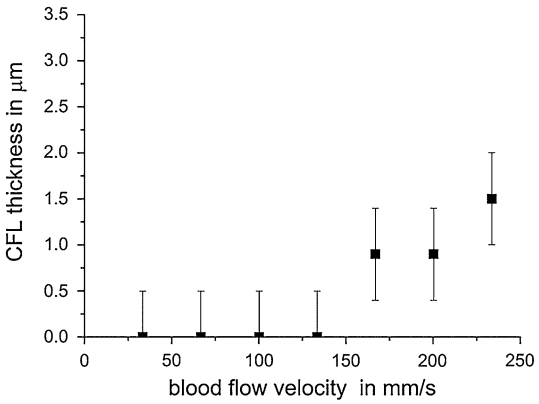

Fig. 12 Thickness of the CFL depending on the blood flow velocity for $hct = 25$ % and evaluation model C

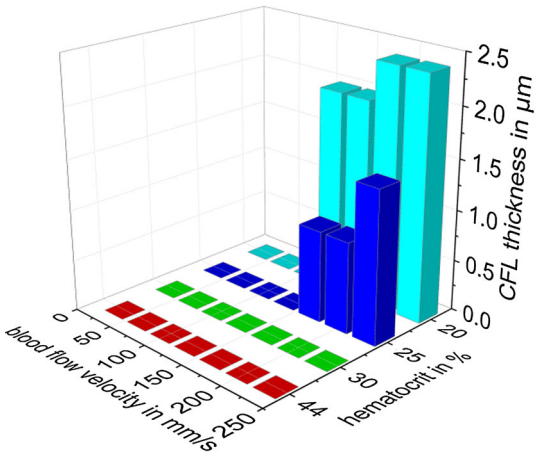

Fig. 13 CFL thickness in dependence of the blood flow velocity and the hematocrit

exchange device of 35 mm/s. The experimental results for all investigated hematocrits and blood flow velocities are summarized in Fig. 13.

8 Conclusion

A novel analysis method was developed to characterize the CFL of blood flowing through a microchannel. In contrast to state-of-the-art methods, the CFL is characterized in the axial z-direction and no special sample preparation is required. Therefore, the laboratory effort is reduced. With the presented method, a minimum CFL thickness of 0.9 µm was detected within in the evaluation model. The results of the characterization are in accordance with the expectations for the presented method and the results of analyzes with comparable settings in other works (Garcia et al. 2012). Since no special sample preparations, such as fluorescence marking of cells or addition of fluorescent microspheres, are necessary, the laboratory effort is reduced significantly. A drawback of the method is the restriction to a minimum thickness of the CFL of 0.9 µm. The CFL is characterized in direction of the optical axis (vertical), which might be advantageous depending on the application. Furthermore, the characterization in whole blood enables more precise results than model fluids. The precision of ±0.5 µm is comparable with or even better than other analyzing methods (Park et al. 2006).

Acknowledgments We thank the Life Imaging Center (LIC) of the University Freiburg, especially Dr. Roland Nitschke and Dr. Angela Naumann, for facilitating the measurements.

References

Campbell NA, Reece JB (2002) Biology, 6th edn. Benjamin Cummings, San Francisco

Cerdeira T, Lima R, Oliveira M, Monteiro FC, Ishikawa T, Imai Y, Yamaguchi T (2009) Determination of the cell-free layer in circular PDMS microchannels. ECCOMAS Thematic Conference on Computational Vision and Medical Image Processing, Porto, Portugal

Fahraeus R, Lindqvist T (1931) The viscosity of the blood in narrow capillary tubes. Am J Physiol Leg Content 96(3):562–568. doi:10.1161/01.RES.22.1.28

Feng J, Hu HH, Joseph DD (1994) Direct simulation of initial value problems for the motion of solid bodies in a Newtonian fluid. Part 1. Sedimentation. J Fluid Mech 261(1):95. doi:10.1017/S0022112094000285

Garcia V, Dias RP, Lima R (2012) In vitro blood flow behaviour in microchannels with simple and complex geometries. In: Naik GR (ed) Applied biological engineering. Principles and practice. InTech, Rijeka, pp 393–416

Karnis A, Goldsmith HL, Mason SG (1966) The flow of suspensions through tubes: V. Inertial effects. Can J Chem Eng 44(4):181–193. doi:10.1002/cjce.5450440401

Lima R, Wada S, Tanaka S, Takeda M, Ishikawa T, Tsubota K, Imai Y, Yamaguchi T (2008) In vitro blood flow in a rectangular PDMS microchannel: experimental observations using a confocal micro-PIV system. Biomed Microdevices 10(2):153–167. doi:10.1007/s10544-007-9121-z

Lima R, Oliveira MS, Ishikawa T, Kaji H, Tanaka S, Nishizawa M, Yamaguchi T (2009) Axisymmetric polydimethysiloxane microchannels for in vitro hemodynamic studies. Biofabrication 1(3):35005. doi:10.1088/1758-5082/1/3/035005

Park CW, Shin SH, Kim GM, Jang JH, Gu YH (2006) A hemodynamic study on a marginal cell depletion layer of blood flow inside a microchannel. KEM 326–328:863–866. doi:10.4028/www.scientific.net/KEM.326-328.863

Rieper T, Wehrstein B, Maurer AN, Mueller C, Reinecke H (2012a) Evaluation model of an extracorporeal gas exchange device made of silicone rubber. Biomed Tech/Biomed Eng 57:1109–1112. doi:10.1515/bmt-2012-4191

Rieper T, Mueller C, Wehrstein B, Maurer AN, Reinecke H (2012a) Virtually monolithic device for diffusive mass transfer enabling high volume flow. In: Proceedings of The Sixteenth International Conference on Miniaturized Systems for Chemistry and Life Sciences (µTAS 2012)

Rieper T, Cvancara P, Gast, Sophie, Wehrstein, Bettina, Maurer, Andreas N., Mueller, Class, Reinecke, Holger (2013) An artificial lung based on gas exchange and blood flow optimization. In: Zengerle R (ed) Proceedings of the 17th International

Conference on Miniaturized Systems for Chemistry and Life Sciences, pp 1188–1190

Segré G, Silberberg A (1962) Behaviour of macroscopic rigid spheres in Poiseuille flow. Part 2 Experimental results and interpretation. J Fluid Mech 14(01):136–157

Tilly de A, Sousa de JM, Willaime H, Pinto JF, Duate Silve OM, Bettencourt Moreira Silva I, Carrapico B, Semiao V (2010) Non-Newtonian micellar microflow visualization in a contraction Geometry. In: Proceedings of the 2nd European Conference on Microfluidics, μFlu'10, Toulouse, France, 08–10 December 2010